Diversity Enhancing Multiple-Mode OFDM With Index Modulation

Qiang Li, Miaowen Wen, *Senior Member, IEEE*, Ertugrul Basar, *Senior Member, IEEE*, H. Vincent Poor, *Fellow, IEEE*, Beixiong Zheng, and Fangjiong Chen, *Member, IEEE*

***Abstract*— As an emerging multi-carrier transmission scheme, multiple-mode orthogonal frequency division multiplexing with index modulation (MM-OFDM-IM) conveys information through multiple distinguishable constellations (or modes, alternatively) and their full permutations, increasing the spectral efficiency of OFDM-IM and classical OFDM. However, both MM-OFDM-IM and its extension, that is, MM-OFDM with in-phase/quadrature index modulation (MM-OFDM-IM-IQ), cannot provide any transmit diversity gain, which may be critical for ultra-reliable communications. In this paper, aiming at enhancing the diversity gain of MM-OFDM-IM(-IQ) schemes, coordinate interleaved (CI-)MM-OFDM-IM and linear constellation precoded (LCP-) MM-OFDM-IM-IQ are proposed, both of which achieve a diversity order of two without loss of spectral efficiency. The optimal rotation angle for CI-MM-OFDM-IM and the optimal precoding matrix for LCP-MM-OFDM-IM-IQ, in the sense of maximizing their coding gains, are derived in closed form. Computer simulations corroborate the advantages of the proposed schemes in terms of diversity and bit error rate performance toward next-generation wireless networks.**

***Index Terms*— OFDM, index modulation, in-phase/quadrature, transmit diversity, the optimal design.**

I. Introduction

INDEX modulation (IM) is a kind of digital modulation technique that utilizes the index(es) of the available transmission entities to convey additional information bits [1], [2]. So far, it has been applied to various systems, including multiple-input multiple-output (MIMO), spread spectrum, and orthogonal frequency division multiplexing (OFDM) systems. Inspired by the early exploration for the frequency-domain IM [3]–[5], Basar *et al.* [6] have proposed an efficient IM-based OFDM scheme, termed OFDM-IM, which activates only a subset of all available subcarriers to carry M-ary data symbols and uses the subcarrier activation patterns (SAPs) as information-bearing units. Besides the optimal maximum-likelihood (ML) detector, the log-likelihood ratio detector that attains near-ML error performance with much lower computational complexity has been designed for OFDM-IM in [6]. Another low-complexity OFDM-IM detector, called greedy detector, has been proposed in [7], which first determines the indices of active subcarriers through measuring subcarrier power and then performs symbol demodulation on those estimated active subcarriers. The error performance of ML and greedy detectors in the presence of channel estimation errors has been studied and compared in [8] and [9], which indicate that in the presence of channel estimation errors, the greedy detector even can offer better error performance than the ML one. Further, various aspects of the achievable performance of OFDM-IM have been studied. For example, with finite constellation input, the achievable rate of OFDM-IM outperforms that of classical OFDM [10]. OFDM-IM also achieves a larger minimum Euclidean distance, which results in better bit error rate (BER) performance at high signal-to-noise ratio (SNR) [11]. Inspired by the superiority of OFDM-IM over classical OFDM, plenty of researchers have launched comprehensive studies on OFDM-IM.

For high data rate and ultra-reliable communications, improving the spectral efficiency (SE) and spatial/frequency diversity of OFDM-IM are two main directions. On the issue of SE, in [12], IM is performed on both the in-phase (I-) and quadrature (Q-) dimensions independently to form OFDM-IM-IQ, while a joint IQ IM scheme is given in [13] and [14] to enhance the SE further. The index domain is expanded to a high-dimensional virtual vector in [15], thus increasing the number of SAPs. MIMO-OFDM-IM combines the MIMO technique and OFDM-IM directly [16], [17]. In [18], a more generic IM scheme is proposed for MIMO-OFDM, where IM is performed not only in the frequency domain but also in the spatial domain. In dual-mode IM-aided OFDM [19], the idle subcarriers of OFDM-IM is also activated and modulated using another constellation. In a more general manner, multiple-mode (MM-)OFDM-IM and MM-OFDM-IM-IQ [20] employ the full permutations of multiple distinguishable constellations within each subblock of subcarriers to carry index bits, increasing both the numbers of symbol and index bits. More recently, an information guided precoding

Manuscript received October 26, 2017; revised January 31, 2018 and March 1, 2018; accepted March 5, 2018. Date of publication March 15, 2018; date of current version August 14, 2018. This work was supported in part by the U.S. National Science Foundation under Grant CCF-1420575, in part by the National Natural Science Foundation of China under Grant 61501190, Grant U1701265, and Grant 61671211, in part by the Natural Science Foundation of Guangdong Province under Grant 2016A030311024, in part by the Pearl River Nova Program of Guangzhou under Grant 201806010171, and in part by the Turkish Academy of Sciences Outstanding Young Scientist Award Programme (TUBA-GEBIP). The associate editor coordinating the review of this paper and approving it for publication was W. Chen. *(Corresponding author: Miaowen Wen.)*

Q. Li, M. Wen, B. Zheng, and F. Chen are with the School of Electronic and Information Engineering, South China University of Technology, Guangzhou 510640, China (e-mail: eeqiangli@mail.scut.edu.cn; emwwen@scut.edu.cn; zheng.bx@mail.scut.edu.cn; eefjchen@scut.edu.cn).

E. Basar is with the Faculty of Electrical and Electronics Engineering, Istanbul Technical University, Istanbul 34469, Turkey (e-mail: basarer@itu.edu.tr).

H. V. Poor is with the Department of Electrical Engineering, Princeton University, Princeton, NJ 08544 USA (e-mail: poor@princeton.edu).

Color versions of one or more of the figures in this paper are available online at http://ieeexplore.ieee.org.

Digital Object Identifier 10.1109/TCOMM.2018.2816058

scheme has been proposed for OFDM using multiple constellations in [21].

On the other hand, since OFDM-IM loses the multipath diversity as classical OFDM, designing spatial/frequency diversity enhancing schemes for OFDM-IM and related systems is very demanding. This paper focuses on this critical topic. Similar to spatial diversity enhancing OFDM schemes [22]–[24], an intuitive way is to deploy multiple receive antennas and adopt diversity reception for OFDM-IM, as suggested in [25]. In [26], an interleaved subcarrier grouping is provided for OFDM-IM to replace the localized subcarrier grouping in order to harvest frequency diversity. In [27], the index bits are transmitted repeatedly through several subblocks with the same SAP, thus achieving a diversity gain for index detection at the cost of SE. A similar idea, in which all active subcarriers are modulated by the identical M-ary data symbols, are investigated in [28] to obtain the frequency diversity for ordinary symbol demodulation. In the scheme of index modulated OFDM spread spectrum [29], a data symbol is spread across several subcarriers by the spreading code that is selected from a predefined set according to the index bits, achieving the diversity order that grows linearly with the subblock size. In [30], the "inactive" subcarriers are reactivated to transmit the same information carried on the active subcarriers by using a different constellation. Space-frequency coded IM for MIMO-OFDM based on the Alamouti codeword is proposed in [31]. In coordinate interleaved OFDM-IM (CI-OFDM-IM) [32], the real and imaginary parts of two complex symbols are interleaved, which ensures that the I- and Q- components of each complex symbol fade separately. The optimal rotation angle for every constellation in [32] is derived through extensive computer search. Inspired by [33] and [34], Wen *et al.* [13] applied the linear constellation precoding (LCP) technique to OFDM-IM-IQ, forming LCP-OFDM-IM-IQ in which the optimal precoding matrix is found by maximizing the coding gain terms contributing to a diversity order of two.

To the best of our knowledge, however, designs of diversity schemes for MM-OFDM-IM(-IQ) [20], which may have potential for ultra-reliable and high-rate communications, have not been investigated. To fill this gap, motivated by CI-OFDM-IM [32] and LCP-OFDM-IM-IQ [13], we design two frequency diversity enhancing schemes in this paper, termed CI-MM-OFDM-IM and LCP-MM-OFDM-IM-IQ, to enhance the asymptotical BER performance of MM-OFDM-IM(-IQ). Both proposed schemes increase the diversity order from unity to two without loss of SE. The main contributions of this paper are summarized as follows:

- An improved closed-form upper bound on the BER of MM-OFDM-IM(-IQ) is derived assuming the ML detection. From the upper bound, we obtain more insights into the diversity achieved by MM-OFDM-IM(-IQ), and explore a method to enhance its diversity gain.
- The technique of CI orthogonal design is first applied to MM-OFDM-IM to form CI-MM-OFDM-IM, in which the I- and Q- components of complex symbols drawn from different constellations are interleaved before each transmission. Hence, each complex symbol is transmitted over two subchannels equivalently. Note that different from [32], the optimal rotation angle for CI-MM-OFDM-IM is analytically derived in closed form and the effects of multiple modes are suitably considered.
- We apply the LCP technique to MM-OFDM-IM-IQ such that within each subset of two subcarriers on each dimension, the symbols are precoded by a precoding matrix after IM. Under the diversity order constraint, the closed-form optimal precoding matrix for LCP-MM-OFDM-IM-IQ in the sense of maximizing their coding gains are obtained. The resulting optimal precoding matrix depends solely on the size of a subblock, which differs from the case in LCP-OFDM-IM-IQ.
- The optimal designs are validated by computer simulations. BER performance of CI-MM-OFDM-IM and LCP-MM-OFDM-IM-IQ is further compared with that of MM-OFDM-IM and MM-OFDM-IM-IQ, where improved diversity gains as well as better BER performance are observed. The schemes of CI-MM-OFDM-IM and LCP-MM-OFDM-IM-IQ are shown to be suitable for systems operating at low and high SEs, respectively.

The rest of this paper is organized as follows. Section II reviews the system model of MM-OFDM-IM(-IQ). Two novel transmit diversity schemes as well as their detection complexity analyses are presented in Section III. Section IV gives the optimal design for the proposed schemes. Section V presents computer simulation results, followed by the conclusion in Section VI.

Notation: Column vectors and matrices are in the form of lowercase and capital bold letters, respectively. Superscripts ^{T} and ^{H} stand for transpose and Hermitian transpose, respectively. $\Re\{\cdot\}$ and $\Im\{\cdot\}$ return the real and imaginary parts of a complex number, respectively. $j = \sqrt{-1}$ denotes the imaginary unit. We use $(\Re\{x\}, \Im\{x\})$ to denote a complex variable x. $\det(\cdot)$ and $\mathrm{rank}(\cdot)$ return the determinant and rank of a matrix, respectively. $\mathrm{diag}(\cdot)$ transforms a vector into a diagonal matrix. $\mathcal{CN}(0, \sigma^2)$ represents the complex Gaussian distribution with zero mean and variance σ^2. The probability of an event and $n \times n$ identity matrix are denoted by $\Pr(\cdot)$ and $\mathbf{I}_n$, respectively. $[a_{11}, a_{12}; a_{21}, a_{22}]$ represents a 2×2 matrix, whose (ι, κ)-th element is $a_{\iota,\kappa}$ for $\iota, \kappa \in \{1, 2\}$. $\|\cdot\|$ denotes the Frobenius norm. $\mathrm{sgn}(\cdot)$ and $\lfloor\cdot\rfloor$ represent the sign and floor functions, respectively.

II. MM-OFDM-IM and MM-OFDM-IM-IQ Revisited

Based on the framework of an OFDM system consisting of N subcarriers, the transmitter structure of MM-OFDM-IM(-IQ) is depicted in Fig. 1. A total of m information bits are split into g subblocks, and each subblock of $p = m/g$ bits is loaded into an index modulator, which is shown in Fig. 2. Each index modulator performs IM within $n = N/g$ subcarriers.[1] As shown in Fig. 2, in MM-OFDM-IM, IM is performed on the complex signal chain, while IM is employed separately on the I- and Q- branches in MM-OFDM-IM-IQ. Next, we outline

[1] In principle, different n values can be chosen for different subblocks. However, using the same n value for all g subblocks leads to the same process in all subblocks, simplifying the practical implementation. Therefore, we adopt the same value of n for all g subblocks in this paper.

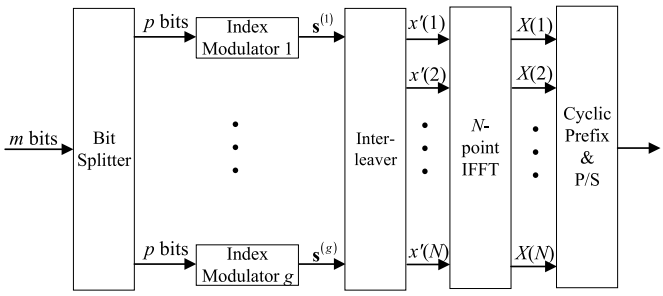

Fig. 1. Transmitter structure of MM-OFDM-IM(-IQ).

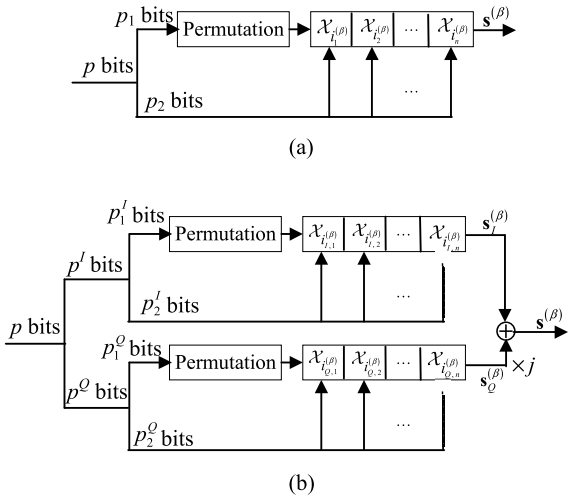

Fig. 2. Index modulator for (a) MM-OFDM-IM and (b) MM-OFDM-IM-IQ within each subblock.

their system models briefly. For both schemes, since the processes in all subblocks are the same and independent of each other, we consider the β-th subblock for illustration without loss of generality, where $\beta \in \{1, \ldots, g\}$.

A. MM-OFDM-IM

As shown in Fig. 2(a), for each subblock, the incoming p bits are divided into two parts for different purposes. The first part, consisting of p_1 index bits, determines the order of the modes $\{\mathcal{X}_1, \ldots, \mathcal{X}_n\}$, forming $\{\mathcal{X}_{i_1^{(\beta)}}, \ldots, \mathcal{X}_{i_n^{(\beta)}}\}$ with the permutation indices $\mathcal{I}^{(\beta)} = [i_1^{(\beta)}, \ldots, i_n^{(\beta)}]^T$, where $i_\gamma^{(\beta)} \in \{1, \ldots, n\}$, and $\mathcal{X}_{i_\gamma^{(\beta)}}$ is an M-ary constellation to be employed by the γ-th subcarrier with $\gamma \in \{1, \ldots, n\}$. We assume that the average power of $\{\mathcal{X}_1, \ldots, \mathcal{X}_n\}$ is normalized to unity. Also, in order to enable IM, $\mathcal{X}_{i_\gamma^{(\beta)}}$ should be distinguishable across γ, which means $\mathcal{I}^{(\beta)}$ is a full permutation of $\{1, \ldots, n\}$. The corresponding n modes $\{\mathcal{X}_1, \ldots, \mathcal{X}_n\}$ can be obtained by partitioning a combined nM-ary constellation $\mathcal{X}$, as described in [20]. For low transceiver and symbol modulation/demodulation complexity, $\mathcal{X}$ is restricted to phase shift keying (PSK) constellations in this paper. Under this constraint, n modes, namely n types of M-PSK, can be easily obtained by rotating the original M-PSK constellation with angles $2\pi(l-1)/nM, l = 1, \ldots, n$. An example for the selection of optimal modes for $n = 4$ and $M = 2$ under the PSK constraint is depicted in Fig. 3. Because of a maximum of $n!$ possible full permutations, it follows that $p_1 = \lfloor \log_2(n!) \rfloor$. The mapping from p_1 bits to $\mathcal{I}^{(\beta)}$ can be realized by either a look-up table or the permutation method. Although this mapping brings about some additional complexity at the transmitter and receiver sides, the incurred complexity is so minor that the additional process would not pose a high computational burden to the transmitter and the receiver. This is because the IM and demodulation are performed within n subcarriers, where n is often a small number, resulting in a small-size look-up table or an easy-to-implement permutation method. Moreover, the processes in all subblocks can be performed in parallel.

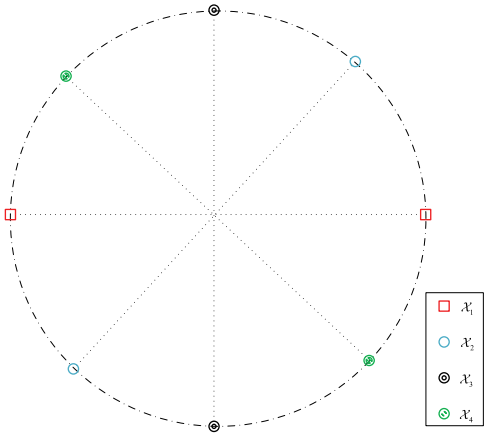

Fig. 3. Optimal mode selection for $n = 4$ and $M = 2$ under the PSK constraint.

According to the obtained $\mathcal{I}^{(\beta)}$ and $\{\mathcal{X}_{i_1^{(\beta)}}, \ldots, \mathcal{X}_{i_n^{(\beta)}}\}$, the second part, consisting of $p_2 = n\log_2(M)$ symbol bits, generates the data symbol vector $\mathbf{s}^{(\beta)} = [s_1^{(\beta)}, \ldots, s_n^{(\beta)}]^T$, where $s_\gamma^{(\beta)} \in \mathcal{X}_{i_\gamma^{(\beta)}}$ for $\gamma = 1, \ldots, n$.

B. MM-OFDM-IM-IQ

As shown in Fig. 2(b), p^I and p^Q bits derived from the incoming p bits are used for IM on the I- and Q- branches, respectively, where $p^I = p^Q$. For the I-branch, similar to the IM method used for MM-OFDM-IM, the p^I bits are separated into $p_1^I = \lfloor \log_2(n!) \rfloor$ index bits and $p_2^I = n\log_2(M)$ symbol bits. According to p_1^I bits and a look-up table or permutation method, the permutation indices $\mathcal{I}_I^{(\beta)} = [i_{I,1}^{(\beta)}, \ldots, i_{I,n}^{(\beta)}]^T$ are determined. Then, the p_2^I bits are mapped to n symbols via n distinguishable M-ary pulse amplitude modulation (PAM) constellations $\{\mathcal{X}_{i_{I,1}^{(\beta)}}, \ldots, \mathcal{X}_{i_{I,n}^{(\beta)}}\}$, forming $\mathbf{s}_I^{(\beta)} = [s_{I,1}^{(\beta)}, \ldots, s_{I,n}^{(\beta)}]^T$, where $s_{I,\gamma}^{(\beta)} \in \mathcal{X}_{i_{I,\gamma}^{(\beta)}}$ and the average power of $\mathcal{X}_{i_{I,\gamma}^{(\beta)}}$ is $1/2$ for $\gamma = 1, \ldots, n$. As described in [20], these n modes $\{\mathcal{X}_{i_{I,1}^{(\beta)}}, \ldots, \mathcal{X}_{i_{I,n}^{(\beta)}}\}$ can be obtained from an nM-PAM constellation. Fig. 4 provides an example for $n = 4$ and $M = 2$.

Following the same IM procedures, with p^Q bits, a symbol vector $\mathbf{s}_Q^{(\beta)}$ on the Q-branch is generated. By combining $\mathbf{s}_I^{(\beta)}$ and $\mathbf{s}_Q^{(\beta)}$, we obtain $\mathbf{s}^{(\beta)} = \mathbf{s}_I^{(\beta)} + j\mathbf{s}_Q^{(\beta)}$.

After obtaining $\{\mathbf{s}^{(\beta)}\}$ for all β, the remaining procedures for both MM-OFDM-IM and MM-OFDM-IM-IQ are the

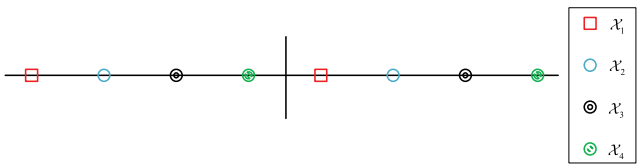

Fig. 4. Optimal mode selection for $n = 4$ and $M = 2$ under the PAM constraint.

same. First, concatenating $\{\mathbf{s}^{(\beta)}\}_{\beta=1}^{g}$ yields the $N \times 1$ main OFDM signal block as follows:

$$\begin{aligned}\mathbf{x} &= \left[\left(\mathbf{s}^{(1)}\right)^T, \ldots, \left(\mathbf{s}^{(g)}\right)^T\right]^T \\ &= \left[s_1^{(1)}, \ldots, s_n^{(1)}, s_1^{(2)}, \ldots, s_n^{(2)}, \ldots, s_1^{(g)}, \ldots, s_n^{(g)}\right]^T. \quad (1)\end{aligned}$$

To harvest the frequency diversity, let (1) pass through a symbol-level interleaver whose output is given by

$$\begin{aligned}\mathbf{x}' &= [x'_1, \ldots, x'_N]^T \\ &= \left[s_1^{(1)}, s_1^{(2)}, \ldots, s_1^{(g)}, \ldots, s_n^{(1)}, s_n^{(2)}, \ldots, s_n^{(g)}\right]^T. \quad (2)\end{aligned}$$

Afterwards, inverse fast Fourier transform (IFFT) is performed on $\mathbf{x}'$ and a cyclic prefix (CP) is added to the beginning of the signal block. Then, parallel-to-serial and digital-to-analog conversions are carried out in sequence. Finally, the resulting signals are transmitted through a frequency-selective Rayleigh fading channel.

At the receiver, after discarding the CP part from the received signal and performing an N-point FFT and the de-interleaving operations, the equivalent input-output relationship for the β-th subblock in the frequency domain is given by

$$\mathbf{y}^{(\beta)} = \left[y_1^{(\beta)}, \ldots, y_n^{(\beta)}\right]^T = \mathbf{X}^{(\beta)}\mathbf{h}^{(\beta)} + \mathbf{w}^{(\beta)}, \quad (3)$$

where $\mathbf{X}^{(\beta)} = \mathrm{diag}(\mathbf{s}^{(\beta)})$, $\mathbf{w}^{(\beta)} = [w_1^{(\beta)}, \ldots, w_n^{(\beta)}]^T$ is a frequency-domain noise vector distributed as $\mathcal{CN}(\mathbf{0}, N_0\mathbf{I}_n)$, and $\mathbf{h}^{(\beta)} = [h_1^{(\beta)}, \ldots, h_n^{(\beta)}]^T$ is the channel vector in the frequency domain. With de-interleaving, $\mathbf{h}^{(\beta)}$ follows the $\mathcal{CN}(\mathbf{0}, \mathbf{I}_n)$ distribution. We define the average SNR per subcarrier as $\rho = 1/N_0$.

Due to the encoding independence between different subblocks, the MM-OFDM-IM(-IQ) signal can be detected block-by-block. From (3), for MM-OFDM-IM, the ML detector for the β-th subblock can be expressed as

$$\left(\hat{\mathbf{s}}^{(\beta)}, \hat{\mathcal{I}}^{(\beta)}\right) = \underset{\mathbf{s}^{(\beta)}, \mathcal{I}^{(\beta)}}{\arg\min} \left\|\mathbf{y}^{(\beta)} - \mathbf{X}^{(\beta)}\mathbf{h}^{(\beta)}\right\|^2, \quad (4)$$

where $\hat{\mathbf{s}}^{(\beta)} \triangleq [\hat{s}_1^{(\beta)}, \ldots, \hat{s}_n^{(\beta)}]^T$ and $\hat{\mathcal{I}}^{(\beta)} \triangleq [\hat{i}_1^{(\beta)}, \ldots, \hat{i}_n^{(\beta)}]^T$.

For MM-OFDM-IM-IQ, the overall detection can be decoupled into independent I- and Q-detections. For the I-branch, as an example, we have

$$\left(\hat{\mathbf{s}}_I^{(\beta)}, \hat{\mathcal{I}}_I^{(\beta)}\right) = \underset{\mathbf{s}_I^{(\beta)}, \mathcal{I}_I^{(\beta)}}{\arg\min} \left\|\mathbf{H}^{(\beta)}\left(\mathbf{z}_I^{(\beta)} - \mathbf{s}_I^{(\beta)}\right)\right\|^2, \quad (5)$$

where $\mathbf{H}^{(\beta)} = \mathrm{diag}(\mathbf{h}^{(\beta)})$ and $\mathbf{z}_I^{(\beta)} = [z_{I,1}^{(\beta)}, \ldots, z_{I,n}^{(\beta)}]^T = \Re\{\mathbf{H}^{(\beta)^{-1}}\mathbf{y}^{(\beta)}\}$ denotes the real part of the equalized received signal.

Obviously, the computational complexities of the optimal ML detectors in (4) and (5), in terms of complex multiplications, are of the same order $\sim \mathcal{O}(n!M^n)$ per subblock.

1) SE: From the above description, the SEs of MM-OFDM-IM and MM-OFDM-IM-IQ without considering the CP overhead are given by (bps/Hz)

$$\mathcal{F}_{\text{MM-OFDM-IM}} = \frac{p_1 + p_2}{n} = \frac{1}{n}\left\lfloor \log_2(n!) \right\rfloor + \log_2(M), \quad (6)$$

and

$$\mathcal{F}_{\text{MM-OFDM-IM-IQ}} = \frac{p^I + p^Q}{n} = \frac{2}{n}\left\lfloor \log_2(n!) \right\rfloor + 2\log_2(M), \quad (7)$$

respectively. From (6) and (7), we conclude that with the same parameters of n and M, the SE of MM-OFDM-IM-IQ doubles that of MM-OFDM-IM.

2) Diversity Order: To get insights into the diversity achieved by MM-OFDM-IM(-IQ), we derive an improved upper bound on the average bit error probability (ABEP) assuming the ML detection. Since the I- and Q- branches are independent in MM-OFDM-IM-IQ, the overall error probability can be represented by the ABEP term contributed by either the I- or Q- branch. Therefore, the ABEP analysis for MM-OFDM-IM and MM-OFDM-IM-IQ is similar. For brevity, we focus only on the ABEP analysis for MM-OFDM-IM and omit the superscript (β) unless otherwise specified.

The error events in MM-OFDM-IM can be categorized into two cases: (i) correct detection of index bits and (ii) incorrect detection of index bits. Hence, it is easy to figure out that ABEP is given by

$$\text{ABEP}_{\text{MM-OFDM-IM}} = \text{ABEP}_{\text{i}} + \text{ABEP}_{\text{ii}}, \quad (8)$$

where

$$\text{ABEP}_{\text{i}} = \frac{p_2}{p} \cdot P_{sb}, \quad (9)$$

and

$$\text{ABEP}_{\text{ii}} \leq \frac{1}{p2^p} \sum_{\substack{\mathbf{X}, \hat{\mathbf{X}} \\ \mathcal{I} \neq \hat{\mathcal{I}}}} \Pr\left(\mathbf{X} \to \hat{\mathbf{X}}\right) G\left(\mathbf{X}, \hat{\mathbf{X}}\right). \quad (10)$$

Note that (10) is obtained from the well-known union bounding technique. The union bound indicates that for any finite or countable set of events, the probability that at least one of the events happens is no greater than the sum of the probabilities of the individual events. A similar formula can also be found in [20]. In (9) and (10),

1) P_{sb} is the ABEP for the M-ary PSK demodulation over Rayleigh fading channels.
2) $\Pr(\mathbf{X} \to \hat{\mathbf{X}})$, which denotes the probability for the event that the transmitted $\mathbf{X}$ is erroneously detected as $\hat{\mathbf{X}}$, is given in [6] by

$$\Pr\left(\mathbf{X} \to \hat{\mathbf{X}}\right) \approx \frac{1/12}{\det\left(\mathbf{I}_n + (\rho/4)\,\mathbf{E}\right)} + \frac{1/4}{\det\left(\mathbf{I}_n + (\rho/3)\,\mathbf{E}\right)}, \quad (11)$$

with $\mathbf{E} = (\mathbf{X} - \hat{\mathbf{X}})^H(\mathbf{X} - \hat{\mathbf{X}})$.

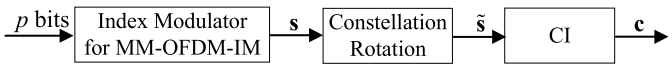

Fig. 5. Index modulator for CI-MM-OFDM-IM within each subblock.

3) $G(\mathbf{X}, \hat{\mathbf{X}})$ is the number of erroneous bits when $\mathbf{X}$ is detected as $\hat{\mathbf{X}}$.

At high SNR, (10) is simplified to

$$\text{ABEP}_{\text{ii}} \leq \frac{1}{12p2^p} \sum_{\substack{\mathbf{X},\hat{\mathbf{X}} \\ \mathcal{I}\neq\hat{\mathcal{I}}}} \left(\prod_{\xi=1}^{r} \lambda_\xi \left(\mathbf{E} \right) \right)^{-1} \times \rho^{-r} \left(4^r + 3^{r+1} \right) G\left(\mathbf{X}, \hat{\mathbf{X}} \right), \quad (12)$$

where $r = \text{rank}(\mathbf{E})$ and $\lambda_\xi(\mathbf{E}), \xi = 1, \ldots, r$, are the nonzero eigenvalues of $\mathbf{E}$. Since in case (ii) at least two modes within each subblock are detected erroneously, we have $r \geq 2$, i.e., the diversity order associated with the index bits detection is two. However, there is no diversity gain in the M-ary symbol demodulation due to the transmission over a single fading channel, which limits the overall diversity of MM-OFDM-IM(-IQ). Fortunately, these observations also point out a method to improve the diversity of MM-OFDM-IM(-IQ).

III. Transmit Diversity Schemes for MM-OFDM-IM(-IQ)

In this section, inspired by the derived ABEP upper bound in (8), we propose two transmit diversity schemes, i.e., CI-MM-OFDM-IM and LCP-MM-OFDM-IM-IQ, for MM-OFDM-IM and MM-OFDM-IM-IQ, respectively, by transmitting each M-ary symbol over multiple fading channels.

A. CI-MM-OFDM-IM

In this subsection, the CI technique is introduced into MM-OFDM-IM to improve its diversity order. The basic principle of CI is to interleave the real and imaginary parts of two complex symbols so that each complex symbol would be transmitted over two subchannels.

The transmitter structure of CI-MM-OFDM-IM is the same as that of MM-OFDM-IM(-IQ) in Fig. 1 except that its index modulator is replaced by the enhanced index modulator of Fig. 5. As shown in Fig. 5, for each subblock, p information bits are first modulated by the index modulator for MM-OFDM-IM, obtaining the symbol vector $\mathbf{s}$. To make CI effective, a constellation rotation is performed on $\mathbf{s}$, yielding $\tilde{\mathbf{s}} = [\tilde{s}_1, \ldots, \tilde{s}_n]^T = e^{j\theta}[s_1, \ldots, s_n]^T$, where $\tilde{s}_\gamma \in \mathcal{X}^\theta_{i_\gamma}, \gamma \in \{1, \ldots, n\}$, and $\theta \in (0, \frac{\pi}{nM})$ is the rotation angle to be optimized. Note that, the combined constellation becomes θ-rotated nM-ary PSK denoted by $\mathcal{X}^\theta$. Constellation rotation is an essential step to ensure that the points in one constellation can be distinguished through one (I- or Q-) dimension [35]. For n being an even number, interleaving the real and imaginary parts of $(\tilde{s}_{2k-1}, \tilde{s}_{2k}), k = 1, \ldots, n/2$, yields

$$\mathbf{c} = \begin{bmatrix} c_1 \\ c_2 \\ \vdots \\ c_{2k-1} \\ c_{2k} \\ \vdots \\ c_{n-1} \\ c_n \end{bmatrix} = \begin{bmatrix} \Re\{\tilde{s}_1\} + j\Im\{\tilde{s}_2\} \\ \Re\{\tilde{s}_2\} + j\Im\{\tilde{s}_1\} \\ \vdots \\ \Re\{\tilde{s}_{2k-1}\} + j\Im\{\tilde{s}_{2k}\} \\ \Re\{\tilde{s}_{2k}\} + j\Im\{\tilde{s}_{2k-1}\} \\ \vdots \\ \Re\{\tilde{s}_{n-1}\} + j\Im\{\tilde{s}_n\} \\ \Re\{\tilde{s}_n\} + j\Im\{\tilde{s}_{n-1}\} \end{bmatrix}. \quad (13)$$

Similar to MM-OFDM-IM, concatenating $\{\mathbf{c}^{(\beta)}\}$ for all β generates the signal vector $\mathbf{x}$ as in (1). The received signal in the frequency domain for the β-th block can be derived in the same form as (3), where $\mathbf{X}^{(\beta)}$ is revised as $\mathbf{X}^{(\beta)} = \text{diag}(\mathbf{c}^{(\beta)})$.

It should be noted that the raw ML detector (4) is also suitable for CI-MM-OFDM-IM. Moreover, due to the CI orthogonal design, the computational complexity of (4) for CI-MM-OFDM-IM can be reduced by single-symbol ML decoding as follows. For each realization of $\mathcal{I}$, denoted by $(\mathcal{I})_\eta, \eta \in \{1, \ldots, 2^{p_1}\}$, the overall ML detection problem can be decomposed into $n/2$ different detection problems, each associated with a pair of symbols $(\tilde{s}_{2k-1}, \tilde{s}_{2k}), k = 1, \ldots, n/2$, which is shown at the bottom of this page as (14). We rewrite (14) in a matrix form as

$$\bar{\mathbf{y}}_k = \bar{\mathbf{H}}_k \left(\bar{\tilde{\mathbf{s}}}_k\right)_\eta + \bar{\mathbf{w}}_k = \left[\bar{\mathbf{H}}_{k,1} \ \bar{\mathbf{H}}_{k,2} \right] \left(\bar{\tilde{\mathbf{s}}}_k\right)_\eta + \bar{\mathbf{w}}_k. \quad (15)$$

For each $\eta \in \{1, \ldots, 2^{p_1}\}$, since the columns of $\bar{\mathbf{H}}_k$ are orthogonal to each other, the ML metric can be calculated as

$$\Delta_\eta = \sum_{k=1}^{n/2} \Bigg(\min_{\tilde{s}_{2k-1} \in \mathcal{X}^\theta_{i_{2k-1}}} \left\| \bar{\mathbf{y}}_k - \bar{\mathbf{H}}_{k,1} \left[\Re\{\tilde{s}_{2k-1}\} \ \Im\{\tilde{s}_{2k-1}\} \right]^T_\eta \right\|^2 + \min_{\tilde{s}_{2k} \in \mathcal{X}^\theta_{i_{2k}}} \left\| \bar{\mathbf{y}}_k - \bar{\mathbf{H}}_{k,2} \left[\Re\{\tilde{s}_{2k}\} \ \Im\{\tilde{s}_{2k}\} \right]^T_\eta \right\|^2 \Bigg). \quad (16)$$

Finally, the receiver determines the permutation indices from

$$\hat{\eta} = \arg\min_{\eta} \Delta_\eta, \quad (17)$$

$$\begin{bmatrix} \Re\{y_{2k-1}\} \\ \Im\{y_{2k-1}\} \\ \Re\{y_{2k}\} \\ \Im\{y_{2k}\} \end{bmatrix} = \begin{bmatrix} \Re\{h_{2k-1}\} & 0 & 0 & -\Im\{h_{2k-1}\} \\ \Im\{h_{2k-1}\} & 0 & 0 & \Re\{h_{2k-1}\} \\ 0 & -\Im\{h_{2k}\} & \Re\{h_{2k}\} & 0 \\ 0 & \Re\{h_{2k}\} & \Im\{h_{2k}\} & 0 \end{bmatrix} \begin{bmatrix} \Re\{\tilde{s}_{2k-1}\} \\ \Im\{\tilde{s}_{2k-1}\} \\ \Re\{\tilde{s}_{2k}\} \\ \Im\{\tilde{s}_{2k}\} \end{bmatrix}_\eta + \begin{bmatrix} \Re\{w_{2k-1}\} \\ \Im\{w_{2k-1}\} \\ \Re\{w_{2k}\} \\ \Im\{w_{2k}\} \end{bmatrix}. \quad (14)$$

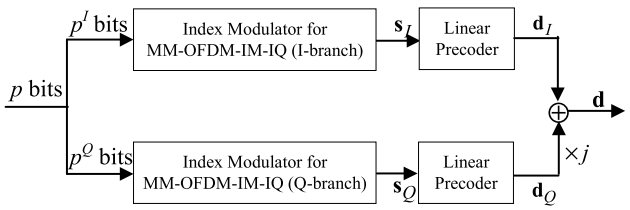

Fig. 6. Index modulator for LCP-MM-OFDM-IM-IQ within each subblock.

and detects the data symbols from

$$\hat{\tilde{s}}_{2k-1} = \underset{\tilde{s}_{2k-1}\in\mathcal{X}^{\theta}_{i_{2k-1}}}{\arg\min} \left\| \bar{\mathbf{y}}_k - \bar{\mathbf{H}}_{k,1}\left[\Re\{\tilde{s}_{2k-1}\}\ \Im\{\tilde{s}_{2k-1}\}\right]^T_{\hat{\eta}} \right\|^2, \tag{18}$$

$$\hat{\tilde{s}}_{2k} = \underset{\tilde{s}_{2k}\in\mathcal{X}^{\theta}_{i_{2k}}}{\arg\min} \left\| \bar{\mathbf{y}}_k - \bar{\mathbf{H}}_{k,2}\left[\Re\{\tilde{s}_{2k}\}\ \Im\{\tilde{s}_{2k}\}\right]^T_{\hat{\eta}} \right\|, \tag{19}$$

for $k = 1, \ldots, n/2$. As seen from (16), the computational complexity of the single-symbol ML detector for CI-MM-OFDM-IM is of order $\sim \mathcal{O}(nn!M)$ per subblock, which is much lower than that of the raw ML detector (4) and increases linearly with n.

B. LCP-MM-OFDM-IM-IQ

The index modulator for LCP-MM-OFDM-IM-IQ is depicted in Fig. 6, which is the same as that of MM-OFDM-IM-IQ except that an additional precoder is employed on each branch. Due to the similarity of encoding and decoding procedures on the I- and Q- dimensions, we focus only on the I-branch in the following.

After obtaining $\mathbf{s}_I$ by using p^I bits, let $\mathbf{s}_I$ pass through the precoder, in which $\mathbf{s}_I$ is decomposed into $n/2$ pairs and each pair is precoded by

$$\mathbf{A} = \begin{bmatrix} a_{11} & a_{12} \\ a_{21} & a_{22} \end{bmatrix}, \tag{20}$$

where all elements are real numbers since PAM symbols are transmitted on both the I- and Q- branches, and we set $a^2_{\iota 1} + a^2_{\iota 2} = 1, \iota = 1, 2$, to ensure the same power as the input. The optimal $\mathbf{A}$ will be investigated in Section IV. After precoding, the output of the precoder becomes

$$\begin{aligned} \mathbf{d}_I &= \begin{bmatrix} d_{I,1} \\ d_{I,2} \\ \vdots \\ d_{I,n-1} \\ d_{I,n} \end{bmatrix} = \begin{bmatrix} \mathbf{A}\begin{bmatrix} s_{I,1} \\ s_{I,2} \end{bmatrix} \\ \vdots \\ \mathbf{A}\begin{bmatrix} s_{I,n-1} \\ s_{I,n} \end{bmatrix} \end{bmatrix} \\ &= \begin{bmatrix} a_{11}s_{I,1} + a_{12}s_{I,2} \\ a_{21}s_{I,1} + a_{22}s_{I,2} \\ \vdots \\ a_{11}s_{I,n-1} + a_{12}s_{I,n} \\ a_{21}s_{I,n-1} + a_{22}s_{I,n} \end{bmatrix}. \end{aligned} \tag{21}$$

Finally, we obtain the transmitted signal by stacking $\mathbf{d}^{(\beta)} = \mathbf{d}_I^{(\beta)} + j\mathbf{d}_Q^{(\beta)}$ for $\beta = 1, \ldots, g$ and implementing the remaining process, which is the same as that for MM-OFDM-IM.

The frequency-domain received signal for the β-th block can be expressed in the same form as (3), where $\mathbf{X}^{(\beta)}$ is revised as $\mathbf{X}^{(\beta)} = \mathrm{diag}(\mathbf{d}^{(\beta)})$. Similar to the detection for MM-OFDM-IM-IQ, the LCP-MM-OFDM-IM-IQ signal can be detected on the I- and Q- branches independently. Specifically, for the I-branch, the ML detection can be formulated as

$$\begin{aligned} \left(\hat{\mathcal{I}}_I, \hat{\mathbf{s}}_I\right) &= \underset{\mathcal{I}_I, \mathbf{s}_I}{\arg\min} \sum_{\gamma=1}^{n} |h_\gamma|^2 |z_{I,\gamma} - d_{I,\gamma}|^2 \\ &= \underset{\mathcal{I}_I}{\arg\min} \sum_{k=1}^{n/2} \min_{\substack{s_{I,2k-1}\in\mathcal{X}_{i_{I,2k-1}} \\ s_{I,2k}\in\mathcal{X}_{i_{I,2k}}}} \sum_{\xi=2k-1}^{2k} |h_\xi|^2 |z_{I,\xi} - d_{I,\xi}|^2, \end{aligned} \tag{22}$$

where $z_{I,\gamma} = \Re\{y_\gamma / h_\gamma\}$, $d_{I,2k-1} = a_{11}s_{I,2k-1} + a_{12}s_{I,2k}$, and $d_{I,2k} = a_{21}s_{I,2k-1} + a_{22}s_{I,2k}$. Let us define

$$D_k = |h_{2k-1}|^2 \left| z_{I,2k-1} - \hat{d}_{I,2k-1} \right|^2 + |h_{2k}|^2 \left| z_{I,2k} - \hat{d}_{I,2k} \right|^2, \tag{23}$$

where $\hat{d}_{I,2k-1}$ and $\hat{d}_{I,2k}$ are estimated from

$$(\hat{s}_{I,2k-1}, \hat{s}_{I,2k}) = \underset{\substack{s_{I,2k-1}\in\mathcal{X}_{i_{I,2k-1}} \\ s_{I,2k}\in\mathcal{X}_{i_{I,2k}}}}{\arg\min} \sum_{\xi=2k-1}^{2k} |h_\xi|^2 |z_{I,\xi} - d_{I,\xi}|^2. \tag{24}$$

Therefore, the ML detection for $\mathcal{I}_I$ in (22) can be performed equivalently by

$$\hat{\mathcal{I}}_I = \underset{\mathcal{I}_I}{\arg\min} \sum_{k=1}^{n/2} D_k. \tag{25}$$

From the above description, in terms of complex multiplications, the computational complexity of the optimal low-complexity ML detection, including the detections for both the I- and Q- branches, is of order $\sim \mathcal{O}(nn!M^2)$ per subblock for LCP-MM-OFDM-IM-IQ.

C. Complexity Comparison

In this subsection, we compare the detection complexity of CI-MM-OFDM-IM and LCP-MM-OFDM-IM-IQ with that of classical OFDM. Table I lists the average number of metric calculations per subcarrier generated by the brute-force ML and low-complexity ML detectors for CI-MM-OFDM-IM, the brute-force ML and low-complexity ML detectors for LCP-MM-OFDM-IM-IQ, and the brute-force ML detector for classical OFDM, which are calculated as $(n-1)!M^n$, $n!M$, $2(n-1)!M^n$, $n!M^2$, and M, respectively. For fair comparisons, we select proper parameters for each scheme to achieve the same SEs of 2, 3, 4, and 6 bps/Hz. As we can observe from Table I, the low-complexity ML detectors for CI-MM-OFDM-IM and LCP-MM-OFDM-IM-IQ exhibit a much lower detection complexity than the brute-force ML detectors, which could be critical for low-latency communications. On the other hand, in comparison with CI-MM-OFDM-IM, LCP-MM-OFDM-IM-IQ offers considerable complexity reduction for either ML or low-complexity ML detection.

TABLE I
COMPARISON OF DETECTION COMPLEXITY BETWEEN CI-MM-OFDM-IM, LCP-MM-OFDM-IM-IQ, AND CLASSICAL OFDM

	CI-MM-OFDM-IM		LCP-MM-OFDM-IM-IQ		Classical OFDM
	ML	Low-Complexity ML	ML	Low-Complexity ML	ML
2 bps/Hz	96 ($n=4, M=2$)	48 ($n=4, M=2$)	N.A.	N.A	2 ($M=2$)
3 bps/Hz	1.54×10^3 ($n=4, M=4$)	96 ($n=4, M=4$)	8 ($n=2, M=2$)	8 ($n=2, M=2$)	8 ($M=8$)
4 bps/Hz	2.46×10^4 ($n=4, M=8$)	192 ($n=4, M=8$)	192 ($n=4, M=2$)	96 ($n=4, M=2$)	16 ($M=16$)
6 bps/Hz	6.29×10^6 ($n=4, M=32$)	768 ($n=4, M=32$)	3.07×10^3 ($n=4, M=4$)	384 ($n=4, M=4$)	64 ($M=64$)

IV. OPTIMAL DESIGN

In this section, under the diversity constraint, we optimize the schemes of CI-MM-OFDM-IM and LCP-MM-OFDM-IM-IQ by maximizing their minimum coding gain distances (CGDs).

A. Optimal Design of CI-MM-OFDM-IM

In CI-MM-OFDM-IM, recalling that $\mathbf{E} = (\mathbf{X} - \hat{\mathbf{X}})^H(\mathbf{X} - \hat{\mathbf{X}})$ and the principle of CI, there are at least two different modulated symbols between $\mathbf{X}$ and $\hat{\mathbf{X}}$, whether the index bits are detected correctly or not. Therefore, we have $r \geq 2$ and the diversity order of CI-MM-OFDM-IM is two. Further, the choice of the rotation angle θ highly affects ABEP. In this subsection, we derive the optimal θ for CI-MM-OFDM-IM in the sense of maximizing the minimum CGD under the constraint $r = 2$, namely,

$$\theta_{opt} = \arg\max_{\theta} \left\{ \min_{\mathbf{X},\hat{\mathbf{X}}} \lambda(\mathbf{E}) \right\}, \tag{26}$$

where $\lambda(\mathbf{E}) = \lambda_1(\mathbf{E})\lambda_2(\mathbf{E})$.

By denoting $\Delta\tilde{s}_\gamma = \tilde{s}_\gamma - \hat{\tilde{s}}_\gamma$ for $\gamma = 1, \ldots, n$, $\mathbf{E}$ can be expressed as

$$\mathbf{E} = \mathrm{diag}\left(\begin{bmatrix} \Re^2\{\Delta\tilde{s}_1\} + \Im^2\{\Delta\tilde{s}_2\} \\ \Re^2\{\Delta\tilde{s}_2\} + \Im^2\{\Delta\tilde{s}_1\} \\ \vdots \\ \Re^2\{\Delta\tilde{s}_{n-1}\} + \Im^2\{\Delta\tilde{s}_n\} \\ \Re^2\{\Delta\tilde{s}_n\} + \Im^2\{\Delta\tilde{s}_{n-1}\} \end{bmatrix} \right). \tag{27}$$

With $r = 2$, without loss of generality, we assume $\Delta\tilde{s}_3 = \cdots = \Delta\tilde{s}_n = 0$, and $(\Delta\tilde{s}_1, \Delta\tilde{s}_2) \neq (0,0)$. Therefore, we have

$$\lambda(\mathbf{E}) = \left(\Re^2\{\Delta\tilde{s}_1\} + \Im^2\{\Delta\tilde{s}_2\}\right)\left(\Re^2\{\Delta\tilde{s}_2\} + \Im^2\{\Delta\tilde{s}_1\}\right). \tag{28}$$

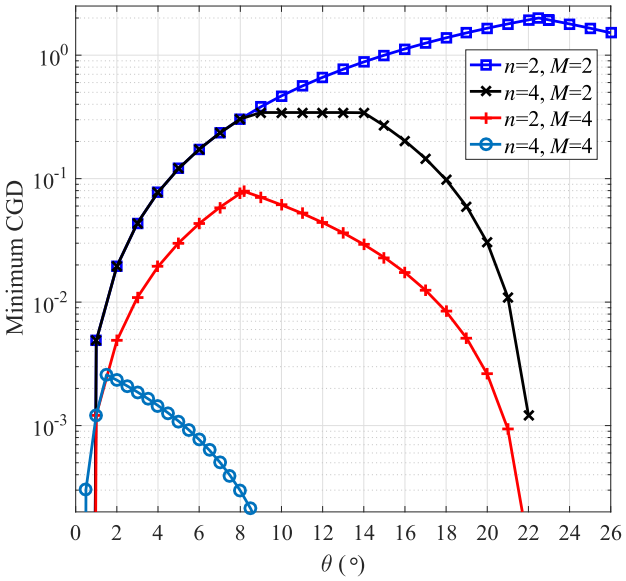

Fig. 7. Minimum CGD versus θ for CI-MM-OFDM-IM.

TABLE II
THE OPTIMAL θ FOR 4 COMBINATIONS OF n AND M

n	M	θ_{opt}
2	2	$22.5°$
4	2	$(8.6°, 13.9°)$
2	4	$8.2°$
4	4	$1.5°$

Proposition 1: The optimal rotation angle θ_{opt} for CI-MM-OFDM-IM is given by (29), shown at the bottom of this page.

Proof: See Appendix A. ■

For example, Table II lists the optimal θ for four combinations of n and M with $n \in \{2, 4\}$ and $M \in \{2, 4\}$. Their minimum CDGs versus θ curves are plotted in Fig. 7, which validate the derived optimal θ values.

$$\theta_{opt} = \begin{cases} \dfrac{\pi}{8}, & \text{for } M = 2, \quad n = 2 \\ \left(\dfrac{1}{2}\arcsin\left(1 - \cos\dfrac{\pi}{n}\right), \dfrac{\pi}{2n} - \dfrac{1}{2}\arcsin\left(1 - \cos\dfrac{\pi}{n}\right)\right), & \text{for } M = 2, \quad n \geq 3 \\ \dfrac{1}{2}\mathrm{arccot}\left(\cot\dfrac{2\pi}{nM} + \dfrac{1 - \cos\dfrac{2\pi}{M}}{2\sin\dfrac{2\pi}{nM}\left(1 - \cos\dfrac{2\pi}{nM}\right)}\right), & \text{for } M \geq 4, \quad n \geq 2. \end{cases} \tag{29}$$

B. Optimal Design of LCP-MM-OFDM-IM-IQ

For the I-branch of LCP-MM-OFDM-IM-IQ, from (21), $\mathbf{E}_I$ is given by

$$\mathbf{E}_I = \left(\mathbf{X}_I - \hat{\mathbf{X}}_I\right)^H \left(\mathbf{X}_I - \hat{\mathbf{X}}_I\right) = \mathrm{diag}\left(\begin{bmatrix} (a_{11}\Delta s_{I,1} + a_{12}\Delta s_{I,2})^2 \\ (a_{21}\Delta s_{I,1} + a_{22}\Delta s_{I,2})^2 \\ \vdots \\ (a_{11}\Delta s_{I,n-1} + a_{12}\Delta s_{I,n})^2 \\ (a_{21}\Delta s_{I,n-1} + a_{22}\Delta s_{I,n})^2 \end{bmatrix}\right), \quad (30)$$

where $\mathbf{X}_I = \mathrm{diag}(\mathbf{d}_I)$ and $\Delta s_{I,\gamma} = s_{I,\gamma} - \hat{s}_{I,\gamma}, \gamma = 1, \ldots, n$.

From (30), we observe that $r \geq 2$ and the equality holds when there is only a pair of symbols $(\Delta s_{I,2k-1}, \Delta s_{I,2k}) \neq (0,0), k \in \{1, \ldots, n/2\}$ and the others are equal to $(0,0)$. Therefore, the diversity order of LCP-MM-OFDM-IM-IQ has been increased to two. However, the precoding matrix $\mathbf{A}$ should be optimized to achieve the maximum coding gain. In this subsection, we address the design problem of the optimal $\mathbf{A}$ for LCP-MM-OFDM-IM-IQ under the constraint $r = 2$. The optimization problem can be formulated as

$$\mathbf{A}_{opt} = \arg\max_{\mathbf{A}} \left\{ \min_{\mathbf{X}_I, \hat{\mathbf{X}}_I} \lambda(\mathbf{E}_I) \right\}, \quad (31)$$
$$s.t. \quad a_{\iota 1}^2 + a_{\iota 2}^2 = 1, \iota = 1, 2,$$

where $\lambda(\mathbf{E}_I) = \lambda_1(\mathbf{E}_I)\lambda_2(\mathbf{E}_I)$.

For the clarity of presentation, we assume $(\Delta s_{I,1}, \Delta s_{I,2}) \neq (0,0)$ and $(\Delta s_{I,2k-1}, \Delta s_{I,2k}) = (0,0)$ for $k = 2, \ldots, n/2$. Thus, we have

$$\lambda(\mathbf{E}_I) = \left[(a_{11}\Delta s_{I,1} + a_{12}\Delta s_{I,2})(a_{21}\Delta s_{I,1} + a_{22}\Delta s_{I,2})\right]^2. \quad (32)$$

For $(\Delta s_{I,1}, \Delta s_{I,2}) \neq (0,0)$, the associated $\lambda(\mathbf{E}_I)$ can be classified into three cases, which are given by (33), shown at the bottom of this page. Therefore, (31) can be further simplified as (34), shown at the bottom of this page.

Lemma: If $\mathbf{A}' = [a'_{11}, a'_{12}; a'_{21}, a'_{22}]$ is a solution to (34), $\mathbf{B} = [\pm|a'_{11}|, \pm|a'_{12}|; \pm|a'_{21}|, \pm|a'_{22}|]$ with $\mathrm{sgn}(b_{11}b_{12}b_{21}b_{22}) = \mathrm{sgn}(a'_{11}a'_{12}a'_{21}a'_{22})$, is also a solution, where $b_{\iota\kappa}$ is the (ι,κ)-th element of $\mathbf{B}$ for $\iota, \kappa \in \{1,2\}$.

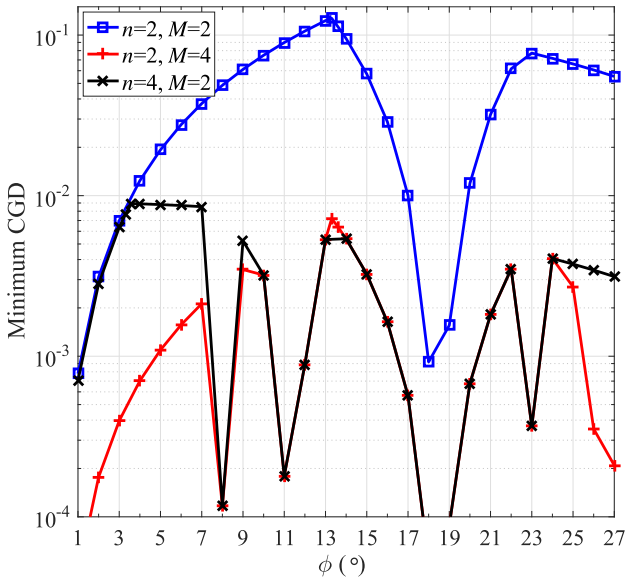

Fig. 8. Minimum CGD versus ϕ for LCP-MM-OFDM-IM-IQ.

Proof: See Appendix B. ■

Proposition 2: The optimal precoder $\mathbf{A}_{opt}$, leading to the maximum CGD, is given by

$$\mathbf{A}_{opt} = \begin{bmatrix} \pm\cos\phi(n) & \pm\sin\phi(n) \\ \pm\sin\phi(n) & \pm\cos\phi(n) \end{bmatrix}, \quad (35)$$

where $a_{11}a_{12}a_{21}a_{22} < 0$ and $\phi(n) = \frac{1}{2}\arctan(\frac{2}{n^2})$.

Proof: See Appendix C. ■

Interestingly, as seen from (35), $\phi(n)$ only depends on n and is independent of M. For example, when $n = 2$ and 4, the optimal values of $\phi(n)$ are 13.3° and 3.6°, respectively, which are also verified by the computer simulations in Fig. 8.

V. Simulation Results and Comparisons

In this section, we perform computer simulations to evaluate the uncoded BER performance of CI-MM-OFDM-IM and LCP-MM-OFDM-IM-IQ by comparing them with MM-OFDM-IM [20], MM-OFDM-IM-IQ [20], OFDM-IM [6], OFDM-IM-IQ [12], and classical OFDM. In all simulations, the number of total OFDM subcarriers is $N = 128$, and each BER point is obtained by averaging over at least 10^5 transmissions. The channel is set to be frequency-selective Rayleigh fading and all considered schemes employ ML or low-complexity ML detection. In OFDM-IM(-IQ), we use n' to denote the number of active subcarriers within n subcarriers.

$$\lambda(\mathbf{E}_I) = \begin{cases} \left[(\Delta s_{I,1})^2 a_{11}a_{21}\right]^2, & \text{for } \Delta s_{I,1} \neq 0, \quad \Delta s_{I,2} = 0 \\ \left[(\Delta s_{I,2})^2 a_{12}a_{22}\right]^2, & \text{for } \Delta s_{I,1} = 0, \quad \Delta s_{I,2} \neq 0 \\ \left[(a_{11}\Delta s_{I,1} + a_{12}\Delta s_{I,2})(a_{21}\Delta s_{I,1} + a_{22}\Delta s_{I,2})\right]^2, & \text{for } \Delta s_{I,1} \neq 0, \quad \Delta s_{I,2} \neq 0. \end{cases} \quad (33)$$

$$\mathbf{A}_{opt} = \arg\max_{\mathbf{A}} \left\{ \min_{\mathbf{X}_I, \hat{\mathbf{X}}_I} \left\{ \left|(\Delta s_{I,1})^2 a_{11}a_{21}\right|, \left|(\Delta s_{I,2})^2 a_{12}a_{22}\right|, \left|(a_{11}\Delta s_{I,1} + a_{12}\Delta s_{I,2})(a_{21}\Delta s_{I,1} + a_{22}\Delta s_{I,2})\right| \right\} \right\}. \quad (34)$$

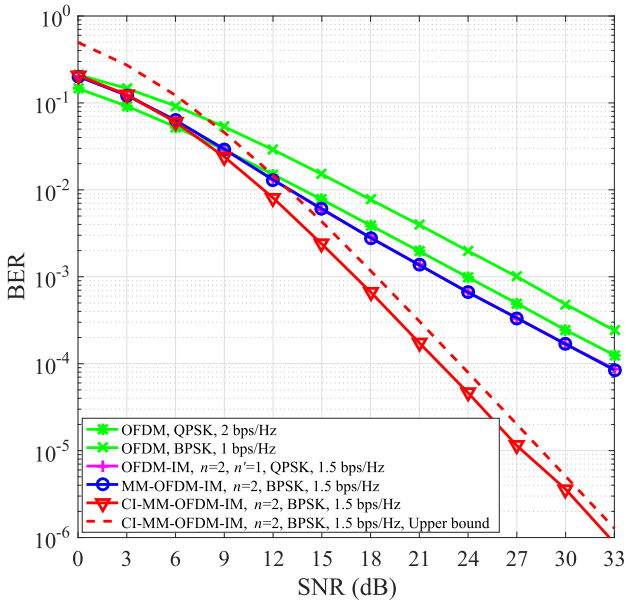

Fig. 9. Performance comparison among classical OFDM, OFDM-IM, MM-OFDM-IM, and CI-MM-OFDM-IM at an SE level of 1.5 bps/Hz.

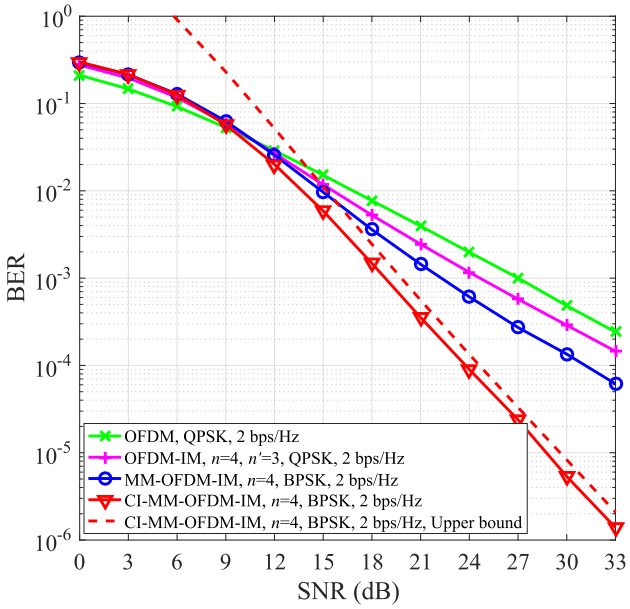

Fig. 10. Performance comparison among classical OFDM, OFDM-IM, MM-OFDM-IM, and CI-MM-OFDM-IM at an SE level of 2 bps/Hz.

A. Perfect Channel Estimation

In this subsection, perfect channel estimation is assumed for all considered schemes. Fig. 9 depicts the comparison results between classical OFDM, OFDM-IM, MM-OFDM-IM, and CI-MM-OFDM-IM, where all schemes achieve an SE of 1.5 bps/Hz except classical OFDM with binary (B-)PSK and QPSK that have SEs of 1 and 2 bps/Hz, respectively. It is worth noting that the comparison is still effective, since the curve of classical OFDM at 1.5 bps/Hz can be predicted to be lying between those at 1 and 2 bps/Hz. As seen from Fig. 9, CI-MM-OFDM-IM achieves a diversity order of two, while other schemes have the same diversity order of unity. Therefore, CI-MM-OFDM-IM performs the best among all schemes when a SNR value is greater than 8 dB. Moreover, the union bound provides an accurate BER prediction for CI-MM-OFDM-IM at high SNR. As revealed in the literature, OFDM-IM exhibits noticeable SNR gains over classical OFDM. Interestingly, given the parameters in this configuration, the BER curve of MM-OFDM-IM overlaps that of OFDM-IM. This can be easily understood by the facts that they transmit the same proportion of the index bits and the power saving provided by OFDM-IM with a factor of 50% stemming from the inactive subcarriers, which corresponds to $10\log_{10}(2) \approx 3$ dB SNR gain, is counterbalanced by the modulation loss from BPSK to QPSK. In general, MM-OFDM-IM outperforms OFDM-IM, which can be observed in the rest of comparisons.

In Fig. 10, we compare the BER performance of classical OFDM, OFDM-IM, MM-OFDM-IM, and CI-MM-OFDM-IM, where all schemes achieve an SE of 2 bps/Hz. As expected, in this system setup, MM-OFDM-IM achieves about 3 dB SNR gain over OFDM-IM at a BER value of 10^{-3}, since the proportion of the index bits in MM-OFDM-IM, which is 1/2, is higher than that in OFDM-IM, which is 1/4. Similar to the observations in Fig. 9, CI-MM-OFDM-IM performs better than all other reference schemes when SNR$\geq$10 dB due to its higher diversity order. Moreover, the upper bound agrees with the computer simulation counterpart well at high SNR.

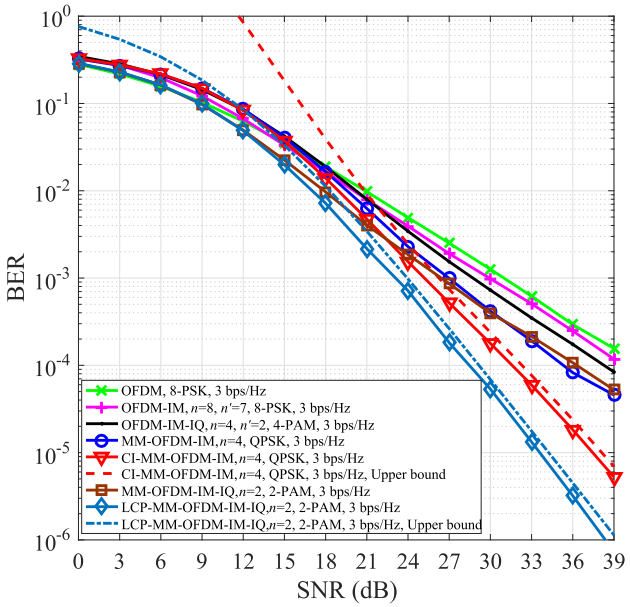

Fig. 11. Performance comparison among classical OFDM, OFDM-IM, OFDM-IM-IQ, MM-OFDM-IM, CI-MM-OFDM-IM, MM-OFDM-IM-IQ, and LCP-MM-OFDM-IM-IQ at an SE level of 3 bps/Hz.

Fig. 11 shows the BER performance of classical OFDM, OFDM-IM, OFDM-IM-IQ, MM-OFDM-IM, CI-MM-OFDM-IM, MM-OFDM-IM-IQ, and LCP-MM-OFDM-IM-IQ, where all schemes achieve an SE of 3 bps/Hz. The BER upper bounds for CI-MM-OFDM-IM and LCP-MM-OFDM-IM-IQ are also given. Similar to the results in [12], OFDM-IM-IQ outperforms OFDM-IM and classical OFDM. In this system setup, we observe that MM-OFDM-IM and MM-OFDM-IM-IQ have similar performance due to their same proportion

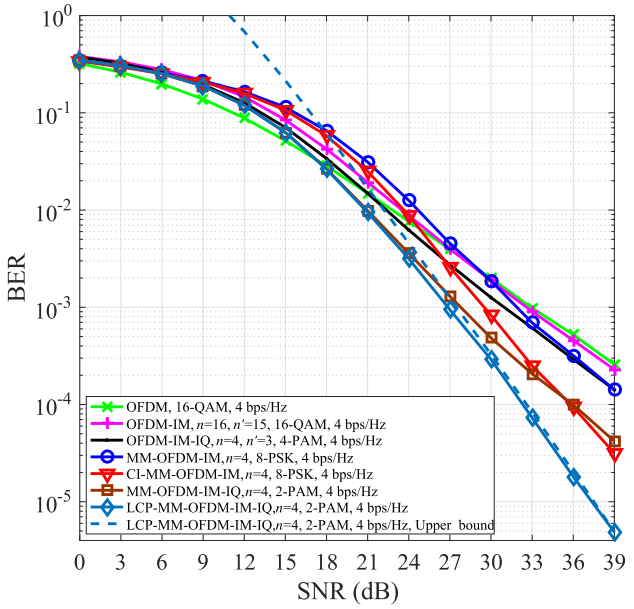

Fig. 12. Performance comparison among classical OFDM, OFDM-IM, OFDM-IM-IQ, MM-OFDM-IM, CI-MM-OFDM-IM, MM-OFDM-IM-IQ, and LCP-MM-OFDM-IM-IQ at an SE level of 4 bps/Hz.

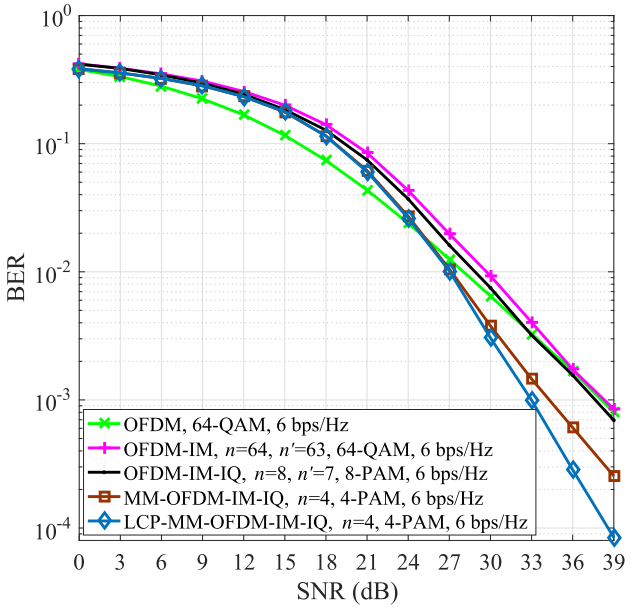

Fig. 13. Performance comparison among classical OFDM, OFDM-IM, OFDM-IM-IQ, MM-OFDM-IM-IQ, and LCP-MM-OFDM-IM-IQ at an SE level of 6 bps/Hz.

of index bits, which is 1/3. However, they still perform slightly different because of the different types of constellations they employ. At low SNR, MM-OFDM-IM-IQ outperforms MM-OFDM-IM, since the minimum distance between different modes in MM-OFDM-IM-IQ, which is $2/\sqrt{10} = 0.6325$, is larger than that in MM-OFDM-IM, which is $\sqrt{2-2\cos\frac{\pi}{8}} = 0.3902$. On the contrary, MM-OFDM-IM-IQ performs worse than MM-OFDM-IM at high SNR. This is because that the minimum distance within each mode in MM-OFDM-IM-IQ, which is given by $4/\sqrt{10} = 0.2649$, is smaller than that in MM-OFDM-IM, which is given by $\sqrt{2} = 1.4142$. As seen from Fig. 11, both CI-MM-OFDM-IM and LCP-MM-OFDM-IM-IQ achieve a diversity order of two, and perform better than MM-OFDM-IM and MM-OFDM-IM-IQ, respectively. On the other hand, LCP-MM-OFDM-IM-IQ obtains approximately a 3 dB SNR gain over CI-MM-OFDM-IM at a BER value of 10^{-5}. Due to the higher complexity and worse BER performance, CI-MM-OFDM-IM is suitable for systems operating at SEs up to 2 bps/Hz, in which LCP-MM-OFDM-IM-IQ is not available.

In Fig. 12, the BER performance of classical OFDM, OFDM-IM, OFDM-IM-IQ, MM-OFDM-IM, CI-MM-OFDM-IM, MM-OFDM-IM-IQ, and LCP-MM-OFDM-IM-IQ are compared at an SE level of 4 bps/Hz. As seen from Fig. 12, MM-OFDM-IM provides little performance improvement with respect to OFDM-IM and classical OFDM, and it even performs worse than OFDM-IM-IQ in the considered SNR range. Although improving the diversity order of MM-OFDM-IM from unity to two, CI-MM-OFDM-IM obtains higher BER values than MM-OFDM-IM-IQ when SNR $\leq$ 36 dB. On the other hand, thanks to the smaller size of constellation employed by each subcarrier and the higher proportion of the index bits, MM-OFDM-IM-IQ achieves an SNR gain of about 4 dB over OFDM-IM-IQ. The same reason explains its

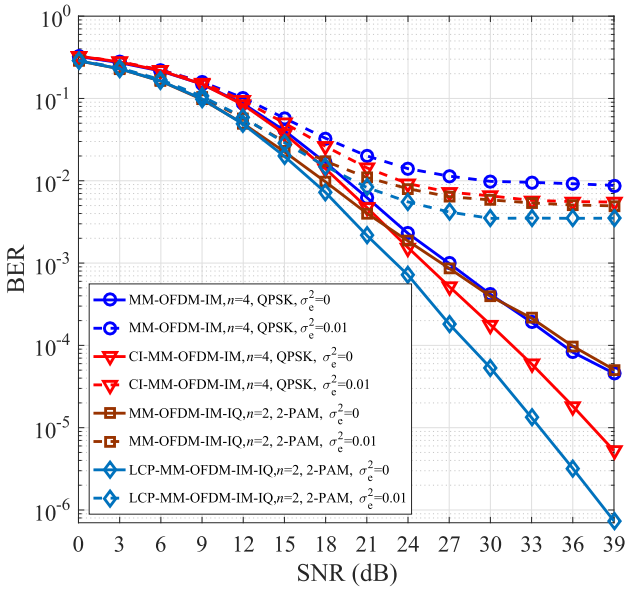

Fig. 14. Performance comparison among MM-OFDM-IM, CI-MM-OFDM-IM, MM-OFDM-IM-IQ, and LCP-MM-OFDM-IM-IQ in the presence of channel estimation errors at an SE level of 3 bps/Hz.

superiority over MM-OFDM-IM. Moreover, we observe from Fig. 12 that LCP-MM-OFDM-IM-IQ performs better than the other schemes, since the diversity improvement in LCP-MM-OFDM-IM-IQ is obtained without loss of SE with respect to MM-OFDM-IM-IQ.

Fig. 13 presents comparison results among classical OFDM, OFDM-IM, OFDM-IM-IQ, MM-OFDM-IM-IQ, and LCP-MM-OFDM-IM-IQ at an SE level of 6 bps/Hz. Through comparing Figs. 11-13, we observe that the superiority of OFDM-IM and OFDM-IM-IQ over classical OFDM becomes marginal with increasing SE. At an SE of 6 bps/Hz, OFDM-IM

even performs worse than classical OFDM in the considered SNR range, as shown in Fig. 13. Fortunately, MM-OFDM-IM-IQ still outperforms OFDM-IM-IQ, OFDM-IM, and classical OFDM at high SEs. With diversity improvement, LCP-MM-OFDM-IM-IQ performs better than MM-OFDM-IM-IQ in the overall SNR region. However, with increasing SE, the superior performance of LCP-MM-OFDM-IM-IQ is only exhibited at higher SNR values. This can be attributed to the larger error probability of detecting the permutation of modes.

B. Imperfect Channel Estimation

In Fig. 14, we compare the BER performance of MM-OFDM-IM, CI-MM-OFDM-IM, MM-OFDM-IM-IQ, and LCP-MM-OFDM-IM-IQ in the presence of channel estimation errors, where all schemes have an SE of 3 bps/Hz and the channel vector $\mathbf{h}$ for each subblock is estimated at the receiver as $\bar{\mathbf{h}} = \mathbf{h} + \mathbf{h}_e$. Here, $\mathbf{h}_e$ represents the vector of channel estimation errors that follows the distribution $\mathcal{CN}(\mathbf{0}, \sigma_e^2 \mathbf{I}_n)$ [36]. As seen from Fig. 14, channel estimation errors deteriorate the BER performance of all schemes and error floors can be observed at high SNR. Moreover, in the presence of channel estimation errors, CI-MM-OFDM-IM and LCP-MM-OFDM-IM-IQ still perform better than conventional MM-OFDM-IM and MM-OFDM-IM-IQ, respectively.

VI. Conclusion

In this paper, we have proposed CI-MM-OFDM-IM and LCP-MM-OFDM-IM-IQ schemes to improve the diversity order of MM-OFDM-IM and MM-OFDM-IM-IQ, respectively. In CI-MM-OFDM-IM, the CI technique is introduced into MM-OFDM-IM, and the real and imaginary parts of two complex symbols from different modes are interleaved. In LCP-MM-OFDM-IM-IQ, the signal vectors on both the I- and Q- branches are precoded by a 2×2 precoder. The optimal rotation angle for CI-MM-OFDM-IM and the optimal precoding coefficients for LCP-MM-OFDM-IM-IQ in the sense of maximizing the minimum CGD have been derived in closed form. Computer simulations have corroborated the optimal design and the diversity improvement achieved by CI-MM-OFDM-IM and LCP-MM-OFDM-IM-IQ. We conclude that the proposed two schemes can be considered as candidates for high data rate and ultra-reliable multi-carrier communication applications.

Appendix A
Proof of Proposition 1

It can be readily figured out that there are two different situations that satisfy $(\Delta\tilde{s}_1, \Delta\tilde{s}_2) \neq (0,0)$. The first situation is that the modes of $\tilde{s}_1$ and $\tilde{s}_2$ are both detected correctly, i.e., $\tilde{s}_\gamma, \hat{\tilde{s}}_\gamma \in \mathcal{X}_{i_\gamma}^{\theta}, \gamma = 1,2$. In this case, errors occur only within modes. The second situation is that the mode of $\tilde{s}_1$ is detected as that of $\tilde{s}_2$ and vice versa.

For the first situation, there are three error cases, namely,

$$\begin{cases} \Delta\tilde{s}_1 \neq 0 \\ \Delta\tilde{s}_2 = 0, \end{cases} \quad \begin{cases} \Delta\tilde{s}_1 = 0 \\ \Delta\tilde{s}_2 \neq 0, \end{cases} \text{ and } \begin{cases} \Delta\tilde{s}_1 \neq 0 \\ \Delta\tilde{s}_2 \neq 0. \end{cases}$$

Due to the symmetry between $\Delta\tilde{s}_1$ and $\Delta\tilde{s}_2$, and the fact that $\Re^2\{\Delta\tilde{s}_1\} \cdot \Im^2\{\Delta\tilde{s}_1\}$ is a term of (28), we only need to consider

$$\lambda(\mathbf{E}) = \Re^2\{\Delta\tilde{s}_1\} \cdot \Im^2\{\Delta\tilde{s}_1\}. \tag{36}$$

With $\tilde{s}_1, \hat{\tilde{s}}_1 \in \mathcal{X}_{i_1}^{\theta}$, we have $\Delta\tilde{s}_1 = \left(\sqrt{2-2\cos\frac{2\pi\upsilon}{M}}\cos\alpha, \sqrt{2-2\cos\frac{2\pi\upsilon}{M}}\sin\alpha\right)$, where $\upsilon \in \{1,\ldots,M-1\}$ and $\alpha \in (0,\pi/2)$ is the angle between $\Delta\tilde{s}_1$ and the x-axis. Hence, (36) leads to

$$\lambda(\mathbf{E}) = \left[\left(1-\cos\frac{2\pi\upsilon}{M}\right)\sin 2\alpha\right]^2. \tag{37}$$

From (37), it can be figured out that

$$\min\{\lambda(\mathbf{E})\} = \left[\left(1-\cos\frac{2\pi}{M}\right)\sin 2\theta\right]^2. \tag{38}$$

For the second situation, two cases, in which (28) may achieve the minimum value, are valid, as described below.

- When $\Delta\tilde{s}_1 = \left(\sqrt{2-2\cos\frac{2\pi}{nM}}\cos\alpha, \sqrt{2-2\cos\frac{2\pi}{nM}}\sin\alpha\right)$ and $\Delta\tilde{s}_2 = -\Delta\tilde{s}_1$, we have
$$\lambda(\mathbf{E}) = \left(2-2\cos\frac{2\pi}{nM}\right)^2. \tag{39}$$
- For $M = 2$, when
$$\Delta\tilde{s}_1 = \left(\sqrt{2-2\cos\frac{\pi(n-1)}{n}}\cos\left(\frac{\pi}{2n}-\theta\right), \sqrt{2-2\cos\frac{\pi(n-1)}{n}}\sin\left(\frac{\pi}{2n}-\theta\right)\right)$$
and
$$\Delta\tilde{s}_2 = \left(\sqrt{2-2\cos\frac{\pi}{n}}\cos\left(\frac{\pi}{2}-\frac{\pi}{2n}+\theta\right), \sqrt{2-2\cos\frac{\pi}{n}}\sin\left(\frac{\pi}{2}-\frac{\pi}{2n}+\theta\right)\right),$$
we have
$$\lambda(\mathbf{E}) = \left[2\sin\left(\frac{\pi}{n}-2\theta\right)\right]^2. \tag{40}$$
For $M \geq 4$, when
$$\Delta\tilde{s}_1 = \left(\sqrt{2-2\cos\frac{2\pi}{nM}}\cos\left(\frac{\pi}{nM}-\theta\right), \sqrt{2-2\cos\frac{2\pi}{nM}}\sin\left(\frac{\pi}{nM}-\theta\right)\right)$$
and
$$\Delta\tilde{s}_2 = \left(\sqrt{2-2\cos\frac{2\pi}{nM}}\sin\left(\frac{\pi}{nM}-\theta\right), \sqrt{2-2\cos\frac{2\pi}{nM}}\cos\left(\frac{\pi}{nM}-\theta\right)\right),$$
we have
$$\lambda(\mathbf{E}) = \left[2\left(1-\cos\frac{2\pi}{nM}\right)\sin\left(\frac{2\pi}{nM}-2\theta\right)\right]^2. \tag{41}$$

$$\theta_{opt} = \begin{cases} \arg\max\limits_{\theta} \left\{ \min \left\{ 2\sin\ 2\theta,\ 2-2\cos\frac{\pi}{n},\ 2\sin\left(\frac{\pi}{n}-2\theta\right) \right\} \right\}, & \text{for } M=2 \\ \arg\max\limits_{\theta} \left\{ \min \left\{ \begin{array}{l} \left(1-\cos\dfrac{2\pi}{M}\right)\sin 2\theta,\ 2-2\cos\dfrac{2\pi}{nM}, \\ 2\left(1-\cos\dfrac{2\pi}{nM}\right)\sin\left(\dfrac{2\pi}{nM}-2\theta\right) \end{array} \right\} \right\}, & \text{for } M \geq 4. \end{cases} \tag{42}$$

By combining (38)-(41), we can formulate (26) as (42), shown at the top of this page.

For $M = 2$, we observe that the curves of $2\sin\ 2\theta$ and $2\sin(\frac{\pi}{n} - 2\theta)$ intersect at $\theta' = \frac{\pi}{4n}$. When $n \geq 3$, we find that $2\sin\ 2\theta' \geq 2 - 2\cos\frac{\pi}{n}$. Hence, for $n \geq 3$, θ_{opt} is an arbitrary angle in the interval $(\frac{1}{2}\arcsin(1-\cos\frac{\pi}{n}), \frac{\pi}{2n} - \frac{1}{2}\arcsin(1-\cos\frac{\pi}{n}))$; for $n = 2$, we have $\theta_{opt} = \frac{\pi}{8}$.

For $M \geq 4$, since $2 - 2\cos\frac{2\pi}{nM} \geq 2(1-\cos\frac{2\pi}{nM})\sin(\frac{2\pi}{nM} - 2\theta)$ for all θ, we have

$$\theta_{opt} = \frac{1}{2}\text{arccot}\left(\cot\frac{2\pi}{nM} + \frac{1-\cos\frac{2\pi}{M}}{2\sin\frac{2\pi}{nM}\left(1-\cos\frac{2\pi}{nM}\right)}\right), \tag{43}$$

from $(1-\cos\frac{2\pi}{M})\sin 2\theta = 2(1-\cos\frac{2\pi}{nM})\sin(\frac{2\pi}{nM} - 2\theta)$. To sum up, we are led to (29).

Appendix B
Proof of Lemma

From (34), CGD is calculated by considering three different cases. The first and the second cases, namely $|(\Delta s_{I,1})^2 a_{11}a_{21}|$ and $|(\Delta s_{I,2})^2 a_{12}a_{22}|$, have the same result for both $\mathbf{A}'$ and $\mathbf{B}$, given the same $\Delta s_{I,1}$ and $\Delta s_{I,2}$. In the third case, with $\text{sgn}(b_{11}b_{12}b_{21}b_{22}) = \text{sgn}(a'_{11}a'_{12}a'_{21}a'_{22})$, for any $\mathbf{A}'$, we can always find an appropriate pair of $\Delta s_{I,1}$ and $\Delta s_{I,2}$ for $\mathbf{B}$ that results in the same value of $|(a_{11}\Delta s_{I,1} + a_{12}\Delta s_{I,2})(a_{21}\Delta s_{I,1} + a_{22}\Delta s_{I,2})|$. In conclusion, $\mathbf{A}'$ and $\mathbf{B}$ generate the same maximum CGD, completing the proof.

Appendix C
Proof of Proposition 2

Due to the symmetry between $\Delta s_{I,1}$ and $\Delta s_{I,2}$, it can be inferred from (34) that $|a_{11}| = |a_{22}|$ and $|a_{12}| = |a_{21}|$. Further, it is sufficient to assume $|a_{11}| > |a_{12}|$ and $|a_{21}| < |a_{22}|$ because swapping a_{11} and a_{12} as well as a_{21} and a_{22} provides the same CGD. From the *Lemma*, we observe that the possible solutions to (34) can be classified into two types, namely $a_{11}a_{12}a_{21}a_{22} > 0$ and $a_{11}a_{12}a_{21}a_{22} < 0$, as the first and second types, respectively.

To begin with, let us consider the first type. According to the *Lemma*, we can only consider $a_{11}, a_{12}, a_{21}, a_{22} > 0$. Let

$$\mathbf{A}_{opt} = \begin{bmatrix} \cos\phi_{opt} & \sin\phi_{opt} \\ \sin\phi_{opt} & \cos\phi_{opt} \end{bmatrix}, \tag{44}$$

where $\phi_{opt} \in (0, \pi/4)$. Note that $s_{I,1}, s_{I,2} \in \{\pm 2, \pm 4, \ldots, \pm 2(nM-1)\}$, the minimum Euclidean distance within a mode is $2n$, and the minimum Euclidean distance between modes is 2. Therefore, (34) can be further simplified as

$$\mathbf{A}_{opt} = \arg\max_{\mathbf{A}} \left\{ \min \left\{ 2n^2 \sin 2\phi_{opt},\ 4\left(1-\sin 2\phi_{opt}\right) \right\} \right\}. \tag{45}$$

In the second type, due to $a_{11}a_{12}a_{21}a_{22} < 0$, without loss of generality, we assume

$$\mathbf{A}_{opt} = \begin{bmatrix} \cos\phi_{opt} & -\sin\phi_{opt} \\ \sin\phi_{opt} & \cos\phi_{opt} \end{bmatrix}. \tag{46}$$

Similar to the first type, with (46), (34) can be expressed as

$$\mathbf{A}_{opt} = \arg\max_{\mathbf{A}} \left\{ \min \left\{ 2n^2 \sin 2\phi_{opt},\ 4\cos 2\phi_{opt} \right\} \right\}. \tag{47}$$

By comparing (45) and (47), we conclude that the maximum CGD is achieved by the second type of $\mathbf{A}_{opt}$ with $2n^2\sin\ 2\phi_{opt} = 4\cos 2\phi_{opt}$, since $4\cos 2\phi > 4(1-\sin\ 2\phi)$ for $\phi \in (0, \pi/4)$. Therefore, we have $\phi(n) = \frac{1}{2}\arctan(\frac{2}{n^2})$, completing the proof.

References

[1] M. Wen, X. Cheng, and L. Yang, *Index Modulation for 5G Wireless Communications*. Berlin, Germany: Springer, 2017.

[2] E. Basar, M. Wen, R. Mesleh, M. Di Renzo, Y. Xiao, and H. Haas, "Index modulation techniques for next-generation wireless networks," *IEEE Access*, vol. 5, pp. 16693–16746, 2017.

[3] R. Abu-alhiga and H. Haas, "Subcarrier-index modulation OFDM," in *Proc. IEEE 20th Int. Symp. Pers., Indoor Mobile Radio Commun. (PIMRC)*, Tokyo, Japan, Sep. 2009, pp. 177–181.

[4] D. Tsonev, S. Sinanovic, and H. Haas, "Enhanced subcarrier index modulation (SIM) OFDM," in *Proc. IEEE Global Commun. Conf. Workshops (GLOBECOM)*, Houston, TX, USA, Dec. 2011, pp. 728–732.

[5] P. K. Frenger and N. A. B. Svensson, "Parallel combinatory OFDM signaling," *IEEE Trans. Commun.*, vol. 47, no. 4, pp. 558–567, Apr. 1999.

[6] E. Basar, U. Aygölü, E. Panayırcı, and H. V. Poor, "Orthogonal frequency division multiplexing with index modulation," *IEEE Trans. Signal Process.*, vol. 61, no. 22, pp. 5536–5549, Nov. 2013.

[7] J. Crawford and Y. Ko, "Low complexity greedy detection method with generalized multicarrier index keying OFDM," in *Proc. IEEE 26th Annu. Int. Symp. Pers., Indoor, Mobile Radio Commun.*, Hong Kong, Aug. 2015, pp. 688–693.

[8] T. V. Luong and Y. Ko, "Impact of CSI uncertainty on MCIK-OFDM: Tight closed-form symbol error probability analysis," *IEEE Trans. Veh. Technol.*, vol. 67, no. 2, pp. 1272–1279, Feb. 2018.

[9] T. V. Luong and Y. Ko, "A tight bound on BER of MCIK-OFDM with greedy detection and imperfect CSI," *IEEE Commun. Lett.*, vol. 21, no. 12, pp. 2594–2597, Dec. 2017.

[10] M. Wen, X. Cheng, M. Ma, B. Jiao, and H. V. Poor, "On the achievable rate of OFDM with index modulation," *IEEE Trans. Signal Process.*, vol. 64, no. 8, pp. 1919–1932, Apr. 2016.

[11] N. Ishikawa, S. Sugiura, and L. Hanzo, "Subcarrier-index modulation aided OFDM—Will it work?" *IEEE Access*, vol. 4, pp. 2580–2593, 2016.

[12] R. Fan, Y. J. Yu, and Y. L. Guan, "Generalization of orthogonal frequency division multiplexing with index modulation," *IEEE Trans. Wireless Commun.*, vol. 14, no. 10, pp. 5350–5359, Oct. 2015.
[13] M. Wen, B. Ye, E. Basar, Q. Li, and F. Ji, "Enhanced orthogonal frequency division multiplexing with index modulation," *IEEE Trans. Wireless Commun.*, vol. 16, no. 7, pp. 4786–4801, Jul. 2017.
[14] R. Fan, Y. J. Yu, and Y. L. Guan, "Improved orthogonal frequency division multiplexing with generalised index modulation," *IET Commun.*, vol. 10, no. 8, pp. 969–974, May 2016.
[15] H. Zhang, L.-L. Yang, and L. Hanzo, "Compressed sensing improves the performance of subcarrier index-modulation-assisted OFDM," *IEEE Access*, vol. 4, pp. 7859–7873, 2016.
[16] E. Basar, "On multiple-input multiple-output OFDM with index modulation for next generation wireless networks," *IEEE Trans. Signal Process.*, vol. 64, no. 15, pp. 3868–3878, Aug. 2016.
[17] B. Zheng, M. Wen, E. Basar, and F. Chen, "Multiple-input multiple-output OFDM with index modulation: Low-complexity detector design," *IEEE Trans. Signal Process.*, vol. 65, no. 11, pp. 2758–2772, Jun. 2017.
[18] T. Datta, H. S. Eshwaraiah, and A. Chockalingam, "Generalized space-and-frequency index modulation," *IEEE Trans. Veh. Technol.*, vol. 65, no. 7, pp. 4911–4924, Jul. 2016.
[19] T. Mao, Z. Wang, Q. Wang, S. Chen, and L. Hanzo, "Dual-mode index modulation aided OFDM," *IEEE Access*, vol. 5, pp. 50–60, 2017.
[20] M. Wen, E. Basar, Q. Li, B. Zheng, and M. Zhang, "Multiple-mode orthogonal frequency division multiplexing with index modulation," *IEEE Trans. Commun.*, vol. 65, no. 9, pp. 3892–3906, Sep. 2017.
[21] Q. Li, M. Wen, H. V. Poor, and F. Chen, "Information guided precoding for OFDM," *IEEE Access*, vol. 5, pp. 19644–19656, 2017.
[22] J. I. Montojo and L. B. Milstein, "Error rate for PSK and QAM modulations for non-ideal OFDM systems with noisy channel estimates and receive diversity," *IEEE Trans. Commun.*, vol. 59, no. 10, pp. 2703–2715, Oct. 2011.
[23] J. Zhang and V. K. N. Lau, "Carrier frequency synchronization and tracking for OFDM systems with receive antenna diversity," *IEEE Trans. Wireless Commun.*, vol. 6, no. 9, pp. 3277–3286, Sep. 2007.
[24] D. Huang, K. B. Letaief, and J. Lu, "A receive space diversity architecture for OFDM systems using orthogonal designs," *IEEE Trans. Wireless Commun.*, vol. 3, no. 3, pp. 992–1002, May 2004.
[25] J. Crawford, E. Chatziantoniou, and Y. Ko, "On the sep analysis of OFDM index modulation with hybrid low complexity greedy detection and diversity reception," *IEEE Trans. Veh. Technol.*, vol. 66, no. 9, pp. 8103–8118, Sep. 2017.
[26] Y. Xiao, S. Wang, L. Dan, X. Lei, P. Yang, and W. Xiang, "OFDM with interleaved subcarrier-index modulation," *IEEE Commun. Lett.*, vol. 18, no. 8, pp. 1447–1450, Aug. 2014.
[27] J. Choi, "Coded OFDM-IM with transmit diversity," *IEEE Trans. Commun.*, vol. 65, no. 7, pp. 3164–3171, Jul. 2017.
[28] T. V. Luong and Y. Ko, "A closed-form symbol error probability for MCIK-OFDM with frequency diversity," in *Proc. IEEE 18th Int. Workshop Signal Process. Adv. Wireless Commun. (SPAWC)*, Hokkaido, Japan, Jul. 2017, pp. 1–5.
[29] Q. Li, M. Wen, E. Basar, and F. Chen, "Index modulated OFDM spread spectrum," *IEEE Trans. Wireless Commun.*, to be published.
[30] J. Zheng and R. Chen, "Achieving transmit diversity in OFDM-IM by utilizing multiple signal constellations," *IEEE Access*, vol. 5, pp. 8978–8988, 2017.
[31] L. Wang, Z. Chen, Z. Gong, and M. Wu, "Space-frequency coded index modulation with linear-complexity maximum likelihood receiver in MIMO-OFDM system," *IEEE Signal Process. Lett.*, vol. 23, no. 10, pp. 1439–1443, Oct. 2016.
[32] E. Basar, "OFDM with index modulation using coordinate interleaving," *IEEE Wireless Commun. Lett.*, vol. 4, no. 4, pp. 381–384, Aug. 2015.
[33] Z. Liu *et al.*, "Linear constellation precoding for OFDM with maximum multipath diversity and coding gains," *IEEE Trans. Commun.*, vol. 51, no. 3, pp. 416–427, Mar. 2003.
[34] N. H. Tran, H. H. Nguyen, and T. Le-Ngoc, "Subcarrier grouping for OFDM with linear constellation precoding over multipath fading channels," *IEEE Trans. Veh. Technol.*, vol. 56, no. 6, pp. 3607–3613, Sep. 2007.
[35] E. Basar, U. Aygolu, E. Panayirci, and H. V. Poor, "A reliable successive relaying protocol," *IEEE Trans. Commun.*, vol. 62, no. 5, pp. 1431–1443, May 2014.
[36] E. Basar, U. Aygolu, E. Panayirci, and H. V. Poor, "Performance of spatial modulation in the presence of channel estimation errors," *IEEE Commun. Lett.*, vol. 16, no. 2, pp. 176–179, Feb. 2012.

Qiang Li received the B.S. degree from the Inner Mongolia University of Science and Technology, Baotou, China, in 2013, and the M.S. degree from the Nanjing University of Aeronautics and Astronautics, Nanjing, China, in 2016. He is currently pursuing the Ph.D. degree with the South China University of Technology, Guangzhou, China. His recent research interests include MIMO systems, index modulation, and OFDM.

Miaowen Wen (M'14–SM'18) received the B.S. degree from Beijing Jiaotong University, Beijing, China, in 2009, and the Ph.D. degree from Peking University, Beijing, China, in 2014. From 2012 to 2013, he was a Visiting Student Research Collaborator with Princeton University, Princeton, NJ, USA. He is currently an Associate Professor with the South China University of Technology, Guangzhou, China. He has authored a book and over 80 papers in refereed journals and conference proceedings. His research interests include index modulation, non-orthogonal multiple access, physical layer security, and molecular communications.

Dr. Wen was a recipient of the Excellent Doctoral Dissertation Award from Peking University in 2014 and the Best Paper Awards from the IEEE International Conference on Intelligent Transportation Systems Telecommunications in 2012, the IEEE International Conference on Intelligent Transportation Systems in 2014, and the IEEE International Conference on Computing, Networking and Communications in 2016. He was an Exemplary Reviewer for the IEEE COMMUNICATIONS LETTERS in 2017. He currently serves as an Associate Editor of the IEEE ACCESS and on the Editorial Board of the *EURASIP Journal on Wireless Communications and Networking*, the *ETRI Journal*, and the *Physical Communication* (Elsevier).

Ertugrul Basar (S'09–M'13–SM'16) received the B.S. degree (Hons.) from Istanbul University, Turkey, in 2007, and the M.S. and Ph.D. degrees from Istanbul Technical University, Turkey, in 2009 and 2013, respectively. From 2011 to 2012, he was with the Department of Electrical Engineering, Princeton University, Princeton, NJ, USA, as a Visiting Research Collaborator. He was an Assistant Professor with Istanbul Technical University from 2014 to 2017, where he is currently an Associate Professor of electronics and communication engineering. He is an inventor of two pending patents on index modulation schemes. His primary research interests include MIMO systems, index modulation, cooperative communications, OFDM, and visible light communications.

Dr. Basar received the Turkish Academy of Sciences Outstanding Young Scientist Award in 2017, the first-ever IEEE Turkey Research Encouragement Award in 2017, and the Istanbul Technical University Best Ph.D. Thesis Award in 2014. He was also a recipient of four best paper awards, including one from the IEEE International Conference on Communications 2016. He is a regular reviewer for various IEEE journals. He currently serves as an Associate Editor for the IEEE COMMUNICATIONS LETTERS and the IEEE ACCESS and an Editor of the *Physical Communication* (Elsevier).

H. Vincent Poor (S'72–M'77–SM'82–F'87) received the Ph.D. degree in EECS from Princeton University in 1977. From 1977 to 1990, he was on the faculty of the University of Illinois at Urbana-Champaign. Since 1990, he has been on the faculty at Princeton, where he is currently the Michael Henry Strater University Professor of Electrical Engineering. From 2006 to 2016, he served as the Dean of Princeton's School of Engineering and Applied Science. He has also held visiting appointments at several other universities, including most recently at Berkeley and Cambridge. His research interests include the areas of information theory and signal processing and their applications in wireless networks, energy systems, and related fields. Among his publications in these areas is the recent book *Information Theoretic Security and Privacy of Information Systems* (Cambridge University Press, 2017).

Dr. Poor is a member of the National Academy of Engineering and the National Academy of Sciences, and is a foreign member of the Chinese Academy of Sciences, the Royal Society, and other national and international academies. He received the Marconi and Armstrong Awards of the IEEE Communications Society in 2007 and 2009, respectively. Recent recognition of his work includes the 2017 IEEE Alexander Graham Bell Medal, the Honorary Professorships at Peking University and Tsinghua University, both conferred in 2017, and a D.Sc. *honoris causa* from Syracuse University also awarded in 2017.

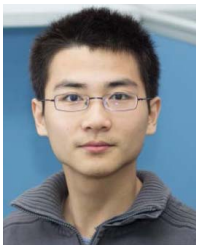

Beixiong Zheng received the B.S. degree from the South China University of Technology, Guangzhou, China, in 2013, where he is currently pursuing the Ph.D. degree. His recent research interests include index modulation, non-orthogonal multiple access, and pilot multiplexing techniques.

From 2015 to 2016, he was a Visiting Student Research Collaborator with Columbia University, New York, NY, USA. He received the Best Paper Award from the IEEE International Conference on Computing, Networking and Communications 2016.

Fangjiong Chen (M'06) received the B.S. degree in electronics and information technology from Zhejiang University, Hangzhou, China, in 1997, and the Ph.D. degree in communication and information engineering from the South China University of Technology, Guangzhou, China, in 2002. He was with the School of Electronics and Information Engineering, South China University of Technology. From 2002 to 2005, he was a Lecturer, and from 2005 to 2011, he was an Associate Professor with the South China University of Technology.

He is currently a full-time Professor with the School of Electronics and Information Engineering, South China University of Technology. He is the Director with the Department of Underwater Detection and Imaging, Mobile Ultrasonic Detection National Research Center of Engineering Technology. His research interests on signal detection and estimation, array signal processing, and wireless communication.

Dr. Chen received the National Science Fund for Outstanding Young Scientists in 2013. He was elected in the New Century Excellent Talent Program of MOE, China, in 2012.